Journal of the Egyptian Mathematical Society 25 (2017) 220–229

Contents lists available at ScienceDirect

Journal of the Egyptian Mathematical Society

journal homepage: www.elsevier.com/locate/joems

Convection instability of non-Newtonian Walter's nanofluid along a vertical layer

Galal M. Moatimid, Mohamed A. Hassan*

Department of Mathematics, Faculty of Education, Ain Shams University, Roxy, Cairo, Egypt

ARTICLE INFO

Article history:
Received 11 May 2016
Revised 5 August 2016
Accepted 29 September 2016
Available online 13 October 2016

JEL classification:
76

Keywords:
Walter's fluid
Linear instability
Nanofluid
Heat transfer

ABSTRACT

The linear stability of viscoelastic nanofluid layer is investigated. The rheological behavior of the viscoelastic fluid is described through the Walter's model. The normal modes analysis is utilized to treat the equations of motion for stationary and oscillatory convection. The stability analysis resulted in a third-degree dispersion equation with complex coefficients. The Routh–Hurwitz theory is employed to investigate the dispersion relation. The stability criteria divide the plane into several parts of stable/unstable regions. This shows some analogy with the nonlinear stability theory. The relation between the elasticity and the longitudinal wave number is graphically analyzed. The numerical calculations show that viscoelastic flows are more stable than those of the Newtonian ones.

1. Introduction

Nanofluids are engineering colloids made of a base fluid and nanoparticles (1–100 nm). The nanofluids have higher thermal conductivity and single-phase heat transfer coefficients than their base fluid [1]. The nanofluids have many various applications including electric chip cooling and coolants for advanced nuclear systems. The physical properties of the base fluid; density, specific heat capacity, thermal conductivity and viscosity are affected by the existence of the nanoparticles. The experimental results for the nanofluid thermo-physical properties were reported in [2]. Applications of nanofluids are being studied in many researches for both the nanofluids with Newtonian or non-Newtonian base through different geometrical shapes. Hayat et al. [3–8] studied the peristaltic transport of nanofluid with Newtonian/non-Newtonian base. The peristaltic transport of nanofluid in a channel with complaint walls was considered with the combined effects of Brownian motion and thermophoretic diffusion of nanoparticles [3]. Meanwhile, the thermal effects of convection, mixed convection and radiation were considered for the peristaltic transport of nanofluids [4–7]. The influences of magnetohydrodynamics (MHD) and thermal radiation on peristaltic transport of a pseudoplastic nanofluid in a tapered asymmetric channel with convective boundary conditions were considered in [4]. It was found that the thermal radiation parameter has a decreasing effect upon heat transfer coefficient. The same authors for the previous Ref. [4] applied the same assumptions of the peristaltic flow to study the Soret and Dufour effects with the existence of chemical reaction [5]. It was found that Soret and Dufour numbers have an opposite effect on the volume fraction and temperature. Also, the thermal radiation on peristaltic transport of nanofluid in a channel satisfying wall properties and convective conditions was investigated in [6]. A quite opposite effect of thermal radiation parameter and the Biot number on the temperature and concentration was found. Two thermal conductivity models were applied, namely the Maxwell's model and the Hamilton–Crosser's model, in Ref. [7]. It was found a quite difference in the results between the two models for higher nanoparticles volume fraction and for nanoparticles with higher thermal conductivity. The non-Newtonian Maxwell nanofluid with mixed convection was analyzed by Hayat et al. [8]. It was found that the thermophoresis parameter enhances the temperature profile and thermal boundary layer thickness. The nanofluid flows over a stretching sheet and disk were studied by Hayat et al. [9,10]. It was shown that the thermophoretic forces enhance the thickness of thermal and nanoparticle volume fraction boundary layers, for the flow over a stretching sheet. Meanwhile, the boundary layer thickness decreases with an increase in the radial stretching of the disk. Convective heat and mass conditions for the non-Newtonian electrically conducting nanofluid flow with the thermal radiation effects were investigated by Hayat et al. [11]. The authors deduced that the thermophoresis and Brownian motion parameters enhance both the temperature and the thermal

* Corresponding author.
E-mail addresses: gal_moa@hotmail.com (G.M. Moatimid), mohamed_gaber@edu.asu.edu.eg (M.A. Hassan).

http://dx.doi.org/10.1016/j.joems.2016.09.001

boundary layer thickness. The stagnation point flow of nanofluid near a permeable stretched surface with convective boundary condition in the presence of porous medium and internal heat generation/ absorption was discussed by Hayat et al. [12]. Also, the effect of thermal radiation on Al_2O_3–water nanofluid flow and heat transfer in an enclosure with a constant heating flux was studied numerically by Hayat et al. [13].

The interaction between the perturbations and the main flow is an important factor in the development of instability for the convective flows. The instability mechanism of the convective flow occurs due to the energy transfer from the main flow to the velocity perturbations, corresponding to the presence of thermal modes. Also, for the convective flow, the unstable stratification of the medium arises due to heating. The instability occurs due to the influence of density, temperature, and gravity inhomogeneities. Therefore, there exists an interaction between the thermal instability and the hydrodynamic perturbations which complicates the problems [14]. The stability of free convective boundary layer flow over a vertical heated flat plate, with respect to two dimensional wave disturbances, was studied by Manosh et al. [15]. They deduced that the external geometry of the fluid domain exerts a considerable influence on stability criteria. Sheu [16] presented a linear stability analysis of the natural convection in a horizontal layer of viscoelastic nanofluid. He deduced that oscillatory instability is possible in both bottom- and top-heavy nanoparticle distributions.

The convective flow of non-Newtonian fluids is of considerable importance in many applications such as; food processing, oil recovery, spread of contaminants in the environment and in many processes in chemical and material industries. The earliest work of studying the instability of non-Newtonian fluids was carried out by Fong and Walters [17]. They found that, according to the infinitesimal disturbance theory, the elasticity destabilizes the flow. But this is not in agreement with some experimental results. Many types of non-Newtonian fluids, such as viscoelastic, Burgers, pseudoplastic, Prandtl, Powell–Eyring, Carreau–Yasuda, Walters-B, Williamson, Jeffrey and Sisko fluids, were studied by Hayat et al. [18–30]. The peristaltic transport of Walters-B fluid in a compliant wall channel in the presence of both velocity and thermal slip conditions were studied in Ref. [18]. Meanwhile, in Ref. [19] the Carreau–Yasuda non-Newtonian model was employed to study the mixed convective peristaltic flow bounded in a compliant wall channel. Also, the Carreau–Yasuda model was employed to study the Hall and MHD effects on peristaltic flow in a convectively curved configuration [20]. The peristaltic flow of Powell–Eyring fluid through curved passage with complaint walls was studied in the presence of viscous dissipation and thermophoresis effects [21]. The authors deduced that the influence of Powell–Eyring fluid parameters on the flow fields is qualitatively opposite. The mixed convective peristaltic flow of Prandtl fluid in a planar channel with compliant walls with the effects of applied magnetic field and Hall current were studied Hayat et al. [22]. A theoretical analysis was presented to study the peristaltic flow and heat transfer characteristics of Burgers' fluid [23]. Also, the same non-Newtonian model, Burgers' fluid, was applied with CattaneoChristov heat flux model of the energy equation instead of Fourier's law of heat conduction [24]. The authors deduced that the temperature distribution is higher in the case of Fourier's law as compared to CattaneoChristov heat flux model. Also, the Cattaneo–Christov heat flux model was applied to investigate the stagnation point flow toward a nonlinear stretched surface with variable thickness and with temperature dependent thermal conductivity [25]. The flow of non-Newtonian magnetic Sisko nanofluid over a bidirectional stretching surface was investigated [26]. The authors illustrated that the effects of Brownian motion and thermophoresis parameters on the nanoparticles concentration distribution are quite opposite. Also, the temperature and nanoparticles concentration distributions are enhanced for the larger values of magnetic parameter. The non-Newtonian pseudoplastic (shear-thinning/shear-thickening) fluid flow through a peristaltic curved channel with the effect of wall properties was studied by Hayat et al. [27]. The results showed that the heat transfer coefficient at the wall is bigger in shear-thinning fluid when compared with the shear-thickening fluid. The homogeneous and heterogeneous reactions in the boundary layer viscoelastic electrically conducting fluid flow over a stretching cylinder with melting heat transfer were investigated in Ref. [28]. It was observed that the heterogeneous reaction parameter decreases the temperature profile. The convective conditions of heat and mass transfer were employed to study the influence of inclined magnetic field on peristaltic flow of an incompressible Williamson fluid in an inclined channel [29]. Also, the mixed convective peristaltic flow of Jeffrey nanofluid in a channel with complaint walls was studied by Hayat et al. [30]. The study included the viscous dissipation, thermal radiation, Joule heating, Hall and ion slip effects.

The recent evolution in the stability analysis of the non-Newtonian fluids is to study the stability of the nanofluids with non-Newtonian base. The linear stability analysis for the Newtonian nanofluid horizontal layer was studied by Nield and Kuznetsov [31]. They found that the primary effect for a typical nanofluid (for which the Lewis number is large) is due to a buoyancy effect coupled with the conservation of nanoparticles. A previous study was developed by Umavathi [32] to study the stability of a viscoelastic nanofluid. He found that the nanofluids have more stabilizing effect when compared by regular fluid. Contributing for the previous studies, Sheu [16] studied the same problem for the nanofluid with the non-Newtonian Oldroyd-B base fluid.

A careful reading of references [16,31,32] has shown that the basic state is taken to be quiescent, which means that the streaming velocity in the basic state is zero. This is logically valid for the horizontal flow, but what happens for the vertical flow? To find the answer for this question, we study the flow of the vertical viscoelastic nanofluid layer. Therefore, the present paper deals with the existing of non-zero stationary streaming velocity. During the following calculations, the stabilizing/destabilizing factors for the problem will be discussed. The Walter's fluid model is employed to describe the rheological behavior of the viscoelastic nanofluid. The Brownian diffusion, thermophoretic diffusion and viscoelasticity effects on the stability criteria are also discussed. In Section 2, the physical description of the problem including the basic equations and the appropriate boundary conditions are presented. Section 3 is devoted to deduce the forms of the basic state for the velocity, temperature and nanoparticles volume fraction. The basic equations of the perturbed state are presented in Section 4. Two cases are considered in Section 5: The first case considers the stability analysis according to the Routh–Hurwitz condition; and the second one concerns the stability analysis due to the stationary and oscillatory states of the dispersion relation. Throughout Section 6, we derived the transition curves and introduce a discussion of the stability pictures according to the elasticity parameter. Finally, in Section 7, we give the concluding remarks for this study based on the obtained results of the stability analysis.

2. Mathematical formulation

Consider an infinite incompressible viscoelastic nanofluid in a vertical layer, subjected to a transverse temperature gradient. The flow is assumed to take place between two vertical boundaries, located at the planes $x=0$ and $x=h$. These plates are considered as heat conductive parallel plates, at which the temperature at the plate $x=0$ is kept at T_1. Meanwhile, the temperature at the plate $x=h$ is held at T_0, where $T_0 \neq T_1$. The rheology of the viscoelastic non-Newtonian fluid is prescribed by the Walter to model the momentum equations. The gravitational acceleration g acts along

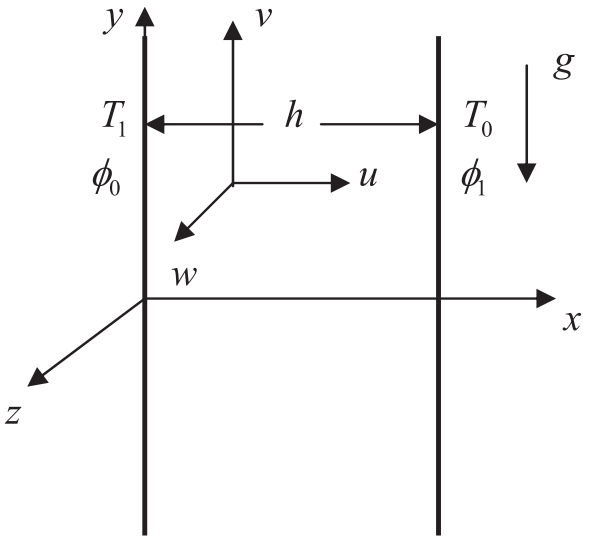

Fig. 1. Physical model and coordinate system.

the negative y-direction. The Cartesian coordinates (x, y, z) are used, where the x-axis is taken normal to the flow channel, y-axis along the vertical flow and z-axis along the horizontal plane. The volumetric fraction of the nanoparticles at the rigid boundaries are considered as constants, namely ϕ_0 and ϕ_1, respectively. Considering constant values of the volume fraction at the boundaries are valid for the basic state according to the constant value of the temperature at the boundaries. A sketch of the physical model is shown in Fig. 1. The Boussinesq approximation is adopted through the problem at hand. The velocity vector $\underline{v}$ is taken as (u, v, w).

The incompressibility condition yields

$$\frac{\partial v_r}{\partial x_r} = 0, \tag{1}$$

According to the work of Buongiorno [1], the momentum equation, in case of the nanofluid, is the same as that of the pure fluid. Taking into account that the spatial variation of the fluid viscosity μ is negligible, the momentum equation according to the Walter's model may be written as [33]

$$\rho_0 \frac{Dv_r}{Dt} = -\frac{\partial P}{\partial x_r} + \mu \frac{\partial^2 v_r}{\partial x_k^2} - \eta \left(\frac{\partial}{\partial t}\left(\frac{\partial^2 v_r}{\partial x_k^2} \right) + v_q \frac{\partial^3 v_r}{\partial x_q \partial x_k^2} - \frac{\partial v_r}{\partial x_q} \frac{\partial^2 v_q}{\partial x_k^2} - 2 \frac{\partial^2 v_r}{\partial x_q \partial x_k} \frac{\partial v_q}{\partial x_k} \right) + \rho g_r, \tag{2}$$

where, $\frac{D}{Dt} = \frac{\partial}{\partial t} + v_k \frac{\partial}{\partial x_k}$ and $g_r = (0, -g, 0)$ is the gravity acceleration vector.

According to the Boussinesq approximation, the thermal conductivity of the nanofluid k is considered as a constant. Therefore, the energy equation may be written in the form [16]

$$(\rho c)_f \left(\frac{DT}{Dt} \right) = k \frac{\partial^2 T}{\partial x_k^2} + (\rho c)_p \left[D_B \left(\frac{\partial \phi}{\partial x_k} \frac{\partial T}{\partial x_k} \right) + \frac{D_T}{T_0} \left(\frac{\partial T}{\partial x_k} \frac{\partial T}{\partial x_k} \right) \right], \tag{3}$$

the volumetric nanoparticle fraction, yields

$$\frac{D\phi}{Dt} = D_B \frac{\partial^2 \phi}{\partial x_k^2} + \frac{D_T}{T_0} \frac{\partial^2 T}{\partial x_k^2}, \tag{4}$$

and the overall density of the nanofluid ρ is given by

$$\rho = [\phi \rho_p + (1 - \phi) \rho_0 (1 - \beta_T (T - T_0))]. \tag{5}$$

where, ρ_p is the particle density, ρ_0 is a reference density of the fluid, β_T is the thermal volumetric expansion, ϕ is the nanoparticle volume fraction, D_B is the Brownian diffusion coefficient, η is the elasticity parameter, P is the pressure, D_T is the thermophoretic diffusion coefficient, c_p is the specific heat of the nanoparticle material, c_f is the specific heat of the fluid, T is the temperature and t is the time.

As stated above, the temperature and the volumetric fraction are assumed constants at the boundaries. Also, the two vertical plates are stationary. So, the no-slip boundary conditions for the velocity, the temperature and the volumetric fraction are:

$$\left.\begin{array}{llll} v = 0, & T = T_1, & \phi = \phi_0, & x = 0 \\ \text{and} & & & \\ v = 0, & T = T_0, & \phi = \phi_1, & x = h \end{array}\right\}, \tag{6}$$

Before dealing with the numerical calculation, it is convenient to rewrite the obtained equations in an appropriate dimensionless form. This can be done in a number of ways depending primarily on the choice of the characteristic length, time and mass. Consider the following dimensionless forms depending on the characteristic length $= h$, the characteristic time $= h^2/\alpha_f$ and the characteristic mass $= \mu h^3/\alpha_f$, where α_f is the thermal diffusivity of the fluid. The other dimensionless quantities are given as follows:

$$\left.\begin{array}{lll} x^* = \frac{x}{h}, & t^* = \frac{t\alpha_f}{h^2}, \quad \alpha_f = \frac{k}{(\rho c)_f}, & v_i^* = \frac{v_i h}{\alpha_f}, \\ P^* = \frac{P h^2}{\mu \alpha_f}, & \phi^* = \frac{\phi - \phi_0}{\phi_1 - \phi_0}, & T^* = \frac{T - \phi_0}{T_1 - \phi_0} \end{array}\right\}. \tag{7}$$

With the aid of Eq. (1), together with the dimensionless quantities as given by Eq. (7), the equations of motion (2–4), after dropping the star for simplicity, may be rewritten as

$$\frac{\partial v_r}{\partial x_r} = 0, \tag{8}$$

$$\frac{1}{Pr} \frac{Dv_r}{Dt} = -\frac{\partial P}{\partial x_r} + \frac{\partial^2 v_r}{\partial x_k^2} - \lambda \left(\frac{\partial}{\partial t}\left(\frac{\partial^2 v_r}{\partial x_k^2} \right) + v_q \frac{\partial^3 v_r}{\partial x_q \partial x_k^2} - \frac{\partial v_r}{\partial x_q} \frac{\partial^2 v_q}{\partial x_k^2} - 2 \frac{\partial^2 v_r}{\partial x_q \partial x_k} \frac{\partial v_q}{\partial x_k} \right) - R_{Mr} + R_{ar} T - R_{Nr} \phi \tag{9}$$

$$\frac{DT}{Dt} = \frac{\partial^2 T}{\partial x_k^2} + \frac{N_B}{Le} \frac{\partial \phi}{\partial x_k} \frac{\partial T}{\partial x_k} + \frac{N_B N_A}{Le} \frac{\partial T}{\partial x_k} \frac{\partial T}{\partial x_k}, \tag{10}$$

and

$$\frac{D\phi}{Dt} = \frac{1}{Le} \frac{\partial^2 \phi}{\partial x_k^2} + \frac{N_A}{Le} \frac{\partial^2 T}{\partial x_k^2}, \tag{11}$$

where, $R_{cr} = (0, R_c, 0)$, and $c = M$, a and N.

Physically, the dilute nanofluid suspension (small value of the nanoparticle volume fraction ϕ) is considered. Also, the temperature gradient is taken as a small quantity. Therefore, the term $\rho_0 \beta_T \phi T$ can be excluded from Eq. (5). It follows the contribution of the term ρg in Eq. (2), which yields the last three terms in Eq. (9) [31].

The other non-dimensional numbers are defined as follows:

- $\mathrm{Pr} = \frac{\mu}{\rho_0 \alpha_f}$, is the Prandtl number.
- $\lambda = \frac{\eta \alpha_f}{h^2 \mu}$, is the elasticity parameter.
- $R_a = \frac{\rho_0 g \beta_T h^3 (T_1 - T_0)}{\mu \alpha_f}$, is the thermal Rayleigh number.
- $R_M = \frac{(\rho_p \phi_0 + \rho_0 (1 - \phi_0)) g h^3}{\mu \alpha_f}$, is the basic density Rayleigh number.
- $R_N = \frac{(\rho_p - \rho_0)(\phi_1 - \phi_0) g h^3}{\mu \alpha_f}$, is the concentration Rayleigh number.
- $N_A = \frac{D_T}{D_B T_0} \frac{(T_1 - T_0)}{(\phi_1 - \phi_0)}$, is the modified diffusivity ratio.
- $N_B = \frac{(\rho c)_p}{\rho_0 c_f} (\phi_1 - \phi_0)$, is the modified particle density increment.

and
$Le = \frac{\alpha_f}{D_B}$, is the Lewis number.

The corresponding boundary conditions, as given in Eq. (6), become

$$\left.\begin{array}{llll} v=0, & T=1, & \phi=0, & x=0 \\ v=0, & T=0, & \phi=1, & x=1 \end{array}\right\}. \tag{12}$$

Now, to study the stability of the system, we assume that the velocity, temperature, volume fraction and the pressure have infinitesimal perturbations from the basic state, such that

$$v_r = v_{rb} + v_r', \; T = T_b + T', \; \phi = \phi_b + \phi' \text{ and } P = P_b + P'. \tag{13}$$

This implies that the basic state of the velocity represents a variable streaming velocity. It is an unknown to be determined during the calculations. In the following sections, we determine the solutions of the basic and perturbed states.

3. The basic state

In the previous studies of the horizontal motion (for example [16,31]), the fluid is considered to be quiescent in the basic state. Physically, this assumption may be true for the horizontal flow. According to the geometry of the present problem, the fluid is flowing vertically due to gravity and then the fluid cannot be considered at rest in the basic state. Therefore, the fluid is flowing in the basic state along y-axis only and the velocity vector becomes v_r=(0, v, 0). According to the continuity Eq. (8), this streaming velocity v must be a function of x only. Also, the temperature and volumetric fraction gradients are along the normal direction to the flow. So, the momentum (Eq. 9) yields,

$$0 = -\frac{\partial P_b}{\partial x}, \tag{14}$$

$$0 = -\frac{\partial P_b}{\partial y} + \frac{d^2 v_b}{dx^2} - R_M + R_a T_b - R_N \phi_b, \tag{15}$$

and

$$0 = -\frac{\partial P_b}{\partial z}. \tag{16}$$

The energy Eq. (10) gives

$$0 = \frac{d^2 T_b}{dx^2} + \frac{N_B}{Le}\frac{d\phi_b}{dx}\frac{dT_b}{dx} + \frac{N_B N_A}{Le}\left(\frac{dT_b}{dx}\right)^2. \tag{17}$$

The volumetric fraction Eq. (11) becomes

$$0 = \frac{1}{Le}\frac{d^2\phi_b}{dx^2} + \frac{N_A}{Le}\frac{d^2 T_b}{dx^2}. \tag{18}$$

The solution of Eqs. (17) and (18) under boundary conditions (12) is in the form

$$T_b = \frac{1 - e^{\frac{N_B}{Le}(1-N_A)(1-x)}}{1 - e^{\frac{N_B}{Le}(1-N_A)}}, \tag{19}$$

and

$$\phi_b = (1 - N_A)x + N_A(1 - T). \tag{20}$$

According to Nield and Kuznetsov [31], most nanofluids have large value for Lewis number Le of order 10^2 to 10^3. Meanwhile, the modified diffusivity ratio N_A is not greater than 10. By analogy, Eqs. (19) and (20) have approximate forms as

$$T_b = 1 - x, \tag{21}$$

$$\phi_b = x. \tag{22}$$

According to Eqs. (14) and (16), the pressure must be a function of y only. So, we can assume that $A = \partial P_b/\partial y$ which is a constant with respect to x. Therefore, the general solution of the basic state velocity in Eq. (15) may be written as

$$v_b = c_1 x + c_2 x^2 + c_3 x^3 \tag{23}$$

where, the constant coefficients $c_1 - c_3$ are given in the Appendix.

4. The perturbed state

To obtain the equations for the perturbed state, we substitute from the solutions of the basic state, Eqs. (21)–(23) into the basic Eqs. (9)–(11). To eliminate the pressure gradient form Eq. (9), we apply curle twice $(curl\, curl)\, \underline{e}_y$ to this equation, (see [16,31,32]). Accordingly, the equations for the perturbed state, in the linear form, and after dropping the dash become

$$\begin{aligned} &\frac{1}{Pr}\left(\frac{\partial}{\partial t}\left(\nabla^2 v\right) + (2c_2 + 6c_3 x)\frac{\partial v}{\partial y} + \left(c_1 x + c_2 x^2 + c_3 x^3\right)\frac{\partial}{\partial y}\left(\nabla^2 v\right)\right) \\ &= \nabla^4 v + R_a \nabla_1^2 T - R_N \nabla_1^2 \phi \\ &\quad - \lambda\left(\frac{\partial}{\partial t}\left(\nabla^4 v\right) + \left(c_1 x + c_2 x^2 + c_3 x^3\right)\frac{\partial}{\partial y}\left(\nabla^4 v\right)\right. \\ &\quad \left. - 2\left(c_1 x + 2c_2 x + 3c_3 x^2\right)\frac{\partial^2}{\partial y\, \partial x_k}\left(\nabla^2 v\right) - 12 c_3 \frac{\partial^2 v}{\partial y\, \partial x_k}\right), \end{aligned} \tag{24}$$

$$\begin{aligned} \frac{\partial T}{\partial t} + \left(c_1 x + c_2 x^2 + c_3 x^3\right)\frac{\partial T}{\partial y} &= \nabla^2 T + \frac{N_B}{Le}\left(\frac{\partial T}{\partial x_k} - \frac{\partial \phi}{\partial x_k}\right) \\ &\quad - 2\frac{N_B N_A}{Le}\frac{\partial T}{\partial x_k}, \end{aligned} \tag{25}$$

and

$$\frac{\partial \phi}{\partial t} + \left(c_1 x + c_2 x^2 + c_3 x^3\right)\frac{\partial \phi}{\partial y} = \frac{1}{Le}\nabla^2 \phi + \frac{N_A}{Le}\nabla^2 T, \tag{26}$$

where $\nabla_1^2 = \frac{\partial^2}{\partial x^2} + \frac{\partial^2}{\partial z^2}$.

We use the previous Eqs. (24)–(26) for the perturbed state in the following section to establish the dispersion relation and hence, to study the stability analysis in the linear case.

5. The linear stability analysis

To determine the dispersion relation of the linear stability, our analysis will base on the normal modes technique. Therefore, all perturbed quantities may be expressed as

$$\begin{pmatrix} v \\ T \\ \phi \end{pmatrix} = \begin{pmatrix} V(x) \\ \theta(x) \\ \Phi(x) \end{pmatrix} e^{i(\ell y + m z + \omega t)}, \tag{27}$$

where, $i = \sqrt{-1}$, ℓ and m are the wave numbers along the y and z-directions and ω is the growth rate. Also, the solutions of $V(x)$, $\theta(x)$ and $\Phi(x)$ that satisfy the boundary conditions Eq. (6) can be written in the form

$$V(x) = v_0 \sin \pi x, \; \theta(x) = \theta_0 \sin \pi x \Phi(x) = \Phi_0 \sin \pi x. \tag{28}$$

Substituting from Eqs. (27) and (28) into Eqs. (24)–(26), and then multiply the resulting equation by $\sin \pi x$. By integrating these equations from x=0 to x=1 and performing some integration by parts, one may set the obtained equations in a matrix

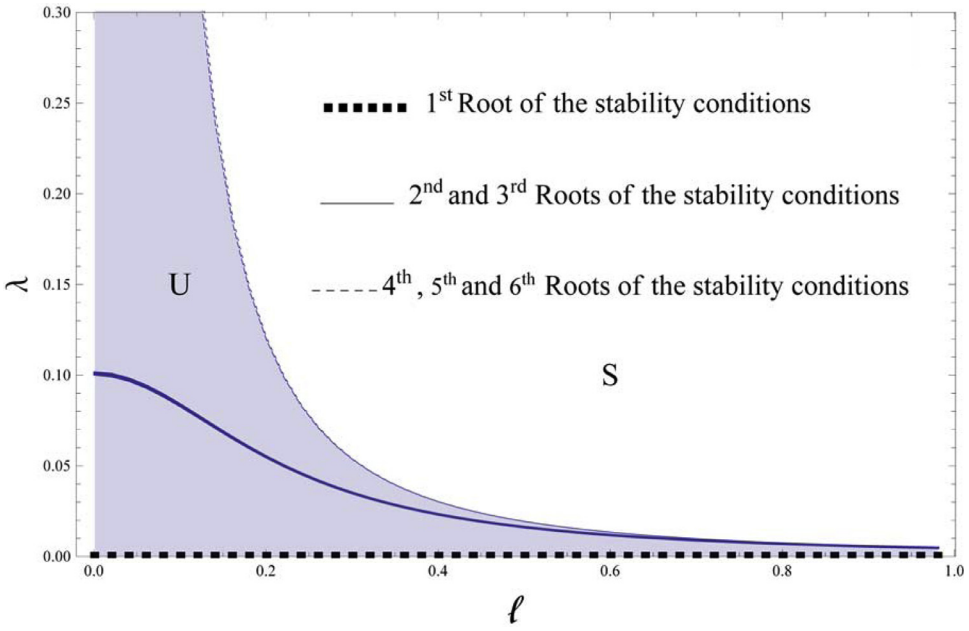

Fig. 2. Stability diagram for a system having the particulars: $Pr=1000$, $Rn=5000$, $Ra=3000$, $Le=100$, $Rm=5000$, $m=0$.

form as given by

$$\begin{pmatrix} M_{11} & -R_a a^2 & R_N a^2 \\ 0 & M_{22} & 0 \\ 0 & \frac{N_A \delta^2}{Le} & M_{33} \end{pmatrix} \begin{pmatrix} v_0 \\ \theta_0 \\ \Phi_0 \end{pmatrix} = \begin{pmatrix} 0 \\ 0 \\ 0 \end{pmatrix}, \tag{29}$$

where, $\delta^2=\pi^2+\ell^2+m^2$ is the total wave number and $a^2=\frac{1}{2}(\pi^2+m^2)$. The other elements, M_{11}, M_{22} and M_{33} are defined in the Appendix.

The nontrivial solution of the Eq. (29) requires that the determinant of coefficients must vanish. Therefore, one directly obtains $M_{11}M_{22}M_{33}=0$, which produces the following dispersion relation

$$h_0\,\omega^3+(h_1+i\,k_1)\,\omega^2+(h_2+i\,k_2)\omega+(h_3+i\,k_3)=0. \tag{30}$$

where, the coefficients k_1-k_3 and h_0-h_3 are given in the Appendix.

According to the normal modes technique as given by Eq. (27), the system becomes stable when the real part of $i\,\omega$ is negative. This corresponds to the case where all roots of ω in Eq. (30) have positive coefficients of the imaginary parts. According to the Routh-Hurwitz theory, the necessary and sufficient stability criteria may be written as [34]

$$\begin{vmatrix} h_0 & h_1 \\ 0 & k_1 \end{vmatrix} < 0, \tag{31}$$

$$\begin{vmatrix} h_0 & h_1 & h_2 & 0 \\ 0 & k_1 & k_2 & 0 \\ 0 & h_0 & h_1 & h_2 \\ 0 & 0 & k_1 & k_2 \end{vmatrix} > 0, \tag{32}$$

and

$$\begin{vmatrix} h_0 & h_1 & h_2 & h_3 & 0 & 0 \\ 0 & k_1 & k_2 & k_3 & 0 & 0 \\ 0 & h_0 & h_1 & h_2 & h_3 & 0 \\ 0 & 0 & k_1 & k_2 & k_3 & 0 \\ 0 & 0 & h_0 & h_1 & h_2 & h_3 \\ 0 & 0 & 0 & k_1 & k_2 & k_3 \end{vmatrix} < 0. \tag{33}$$

The previous three conditions, in Eqs. (31)–(33), govern the linear stability conditions. The numerical calculations of these conditions divide the plane into several parts of stable/unstable regions. The stable regions occur when these conditions are simultaneously satisfied. Meanwhile, invalidation for one of these conditions (at least) gives an unstable region. This shows some analogy with the nonlinear stability theory. These conditions will be represented graphically to discuss the stabilizing parameters in the next section.

Another algorithm to study the stability criteria is to determine the stationary and oscillatory states from the dispersion relation Eq. (30). To do this, we assume that $\omega=i\,\omega_i$, then collecting the real and imaginary parts according to the coefficients of the elasticity parameter λ in the dispersion relation (30) to obtain the following form

$$\lambda=\frac{(\Delta_3+i\,\Delta_4)}{(\Delta_1+i\,\Delta_2)}, \tag{34}$$

where,

$$\Delta_1=n_1\,\omega_i^3-n_2\,\omega_i^2-n_3\,\omega_i+n_4,$$
$$\Delta_2=-n_5\,\omega_i^2+n_6\,\omega_i+n_7,$$
$$\Delta_3=-m_1\,\omega_i^3+m_2\,\omega_i^2+m_3\,\omega_i-m_4,$$

and

$$\Delta_4=m_5\,\omega_i^2-m_6\,\omega_i-m_7.$$

where, the coefficients n_1-n_7 and m_1-m_7 are defined in the Appendix.

The steady convection state occurs at $\omega_i=0$, then the dispersion relation given in Eq. (34) tends to the form

$$\lambda^S=\left(\frac{-n_4m_4-n_7m_7}{n_4^2+n_7^2}\right)+i\left(\frac{-n_4m_7+n_7m_4}{n_4^2+n_7^2}\right). \tag{35}$$

The elasticity parameter λ must be real. So, the imaginary part of the previous Eq. (35) must vanish. This gives the equation $n_7m_4-n_4m_7=0$. The simplification of this equation gives a common factor bracket which tends to a restriction on the pressure gradient in the form

$$A=\frac{1}{2}(R_a-2R_M-R_N). \tag{36}$$

The application of the previous restriction, during the calculations for the stability conditions [31–33], gives real values only

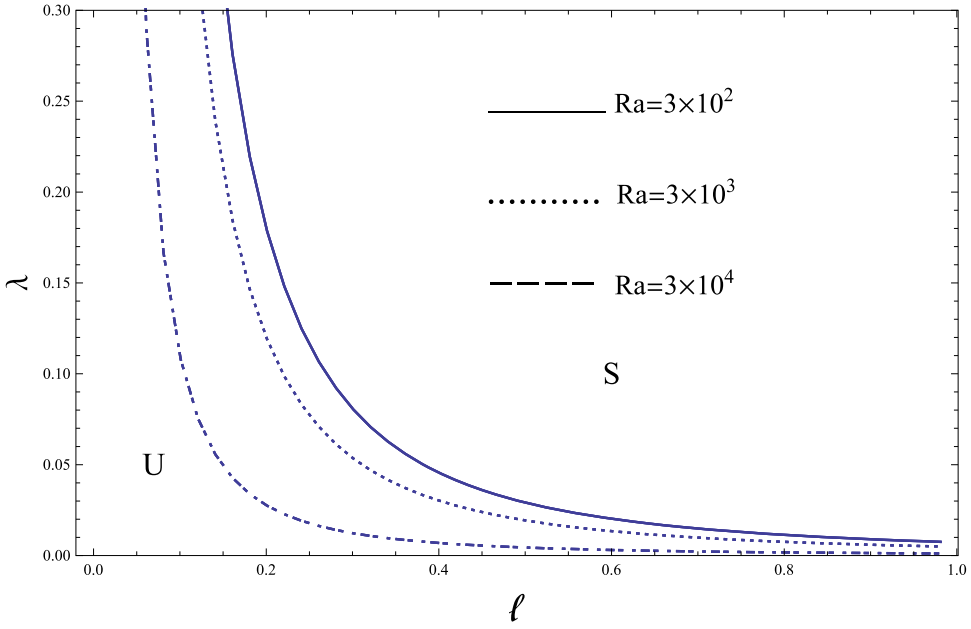

Fig. 3. Stability diagram for a system having the particulars: $Pr=1000$, $Rn=5000$, $Le=100$, $Rm=5000$, $m=0$.

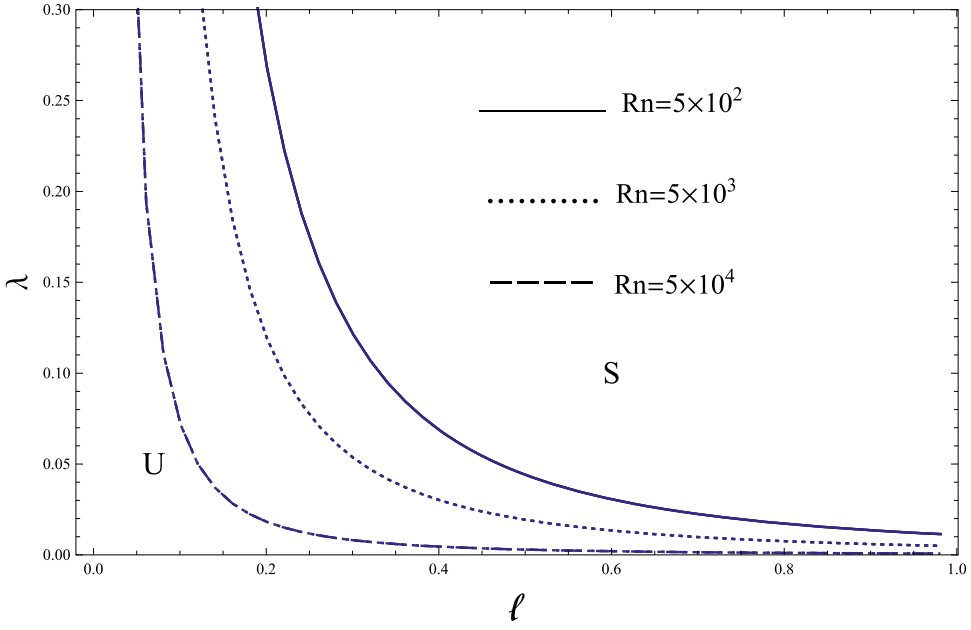

Fig. 4. Stability diagram for a system having the particulars: $Pr=1000$, $Ra=3000$, $Le=100$, $Rm=5000$, $m=0$.

for all roots of the stability conditions. This will discuss in details in the next section. Meanwhile, the oscillatory state occurs for $\omega_i \neq 0$. By taking the real part only from Eq. (34), the dispersion relation of the oscillatory states can be written as

$$\lambda^{OSC} = \frac{\Delta_1\Delta_3 + \Delta_2\Delta_4}{\Delta_1^2 + \Delta_2^2}. \tag{36}$$

Graphically, the departure of the curve from the steady state means a destabilizing effect of the parameter. This will be illustrated in the next section graphically.

6. Results and discussion

Through this section, we shall discuss the stability criteria graphically. Our discussions are dividing into two categories. Firstly, the stability criteria, that is depending on the Routh–Hurwitz conditions in Eqs. (31)–(33), is discussed. Secondly, the stability is discussed depending on the graphical representation of the steady and oscillatory states of the elasticity parameter in Eqs. (35) and (36).

One of the main aims of the present study is to discuss the non-Newtonian rheology effect according to the elasticity parameter. Therefore, we confine our attention to graph the relation between the elasticity parameter λ and the wave number in the longitudinal direction ℓ. The expansion of the determinant in Eq. (31) gives a second order equation of λ and for the determinant in Eq. (32) gives a fourth degree equation of λ. Meanwhile, the determinant in Eq. (33) produces a sixth order equation of λ. It is expected that some of the roots of these equations are real and the others are imaginary. The application of the restriction

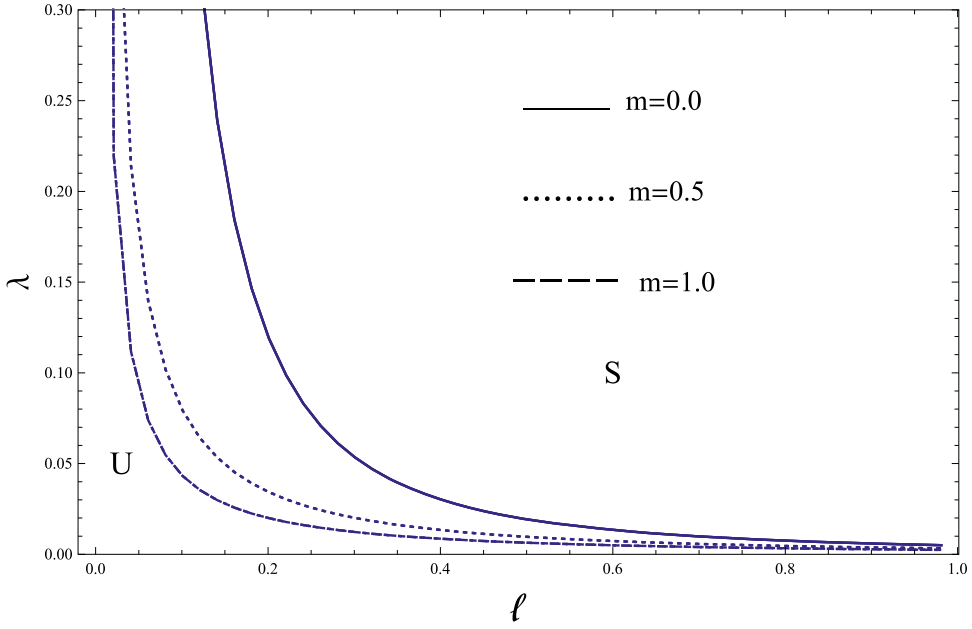

Fig. 5. Stability diagram for a system having the particulars: $Pr=1000$, $Rn=5000$, $Ra=3000$, $Le=100$, $Rm=5000$.

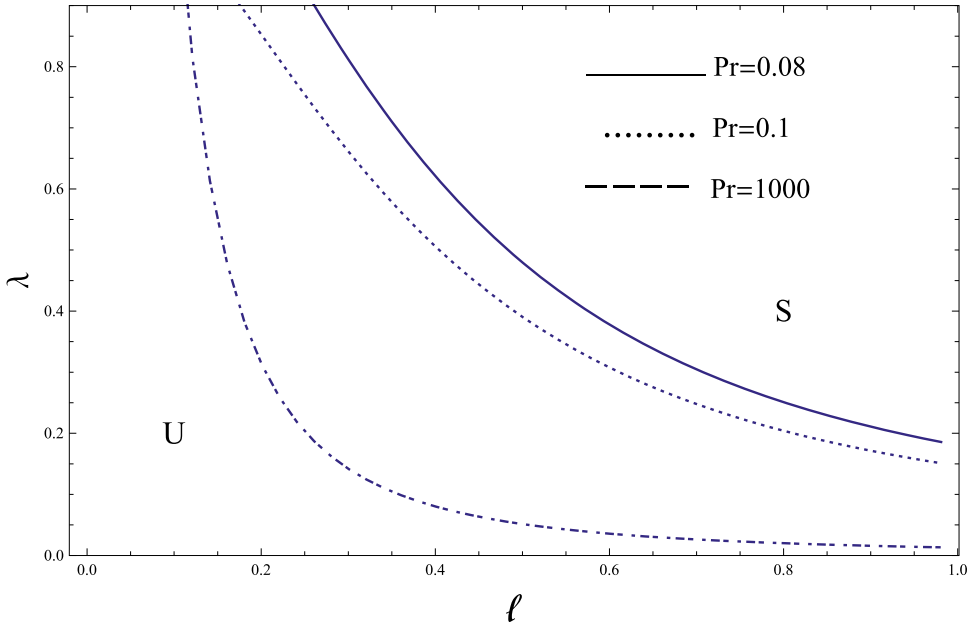

Fig. 6. Stability diagram for a system having the particulars: $Rn=0.3$, $Ra=3000$, $Le=100$, $Rm=5000$, $m=0$.

in Eq. (36) during the calculations induces real roots only for all conditions (31)–(33).

In Fig. 2, the neutral curves of the linear stability conditions (31)–(33) divide the plane into a stable region and an unstable region. The region symbolized *S* refers the stabilized region, while the region symbolized *U* is a destabilized region. The dotted line represents the first root for all conditions (31)–(33). The region under this curve is a stable region according to the inequalities (31)–(33). This implies that the stable region under the dotted curve is a very thin negligible layer represents the range $0 < \lambda \leq 10^{-4}$ of the elasticity parameter. This means that the stability enhances in case of nanofluid with non-Newtonian base. Meanwhile, this mechanism dose not appears for the case of nanofluid with Newtonian base. The solid curve in Fig. 2 represents the second and third roots for all conditions (31)–(33). Meanwhile, the dashed curve represents the fourth root of the condition (32) and the fifth and sixth roots of condition (33). The shaded region under the dashed curve represents an unstable region. This occurs due to unsatisfying the stability conditions (31)–(33) simultaneously. So, for the small range of the elasticity parameter (the unstable region in the figure), instability is of hydrodynamic nature due to the development of vortices between countercurrent flows.

Fig. 3 illustrates the effect of thermal Rayleigh number on the stability picture. One can see that the thermal Rayleigh number stabilizes the nanofluid layer according to the increasing of the stability region with increasing the Rayleigh number. Similar result was obtained by Sheu [16], where the stationary convection state was obtained by increasing the Rayleigh number.

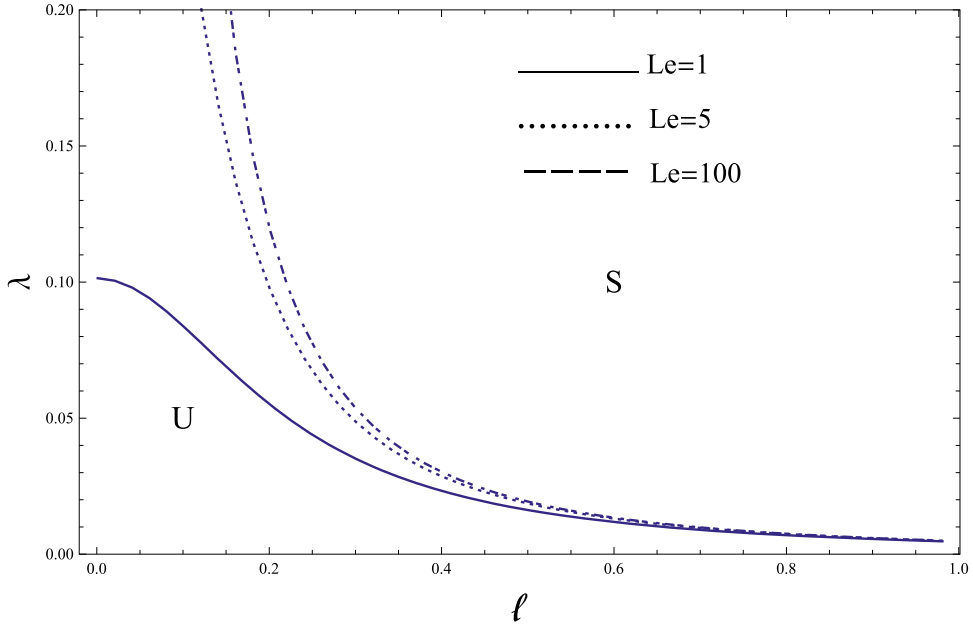

Fig. 7. Stability diagram for a system having the particulars: $Pr=1000$, $Rn=5000$, $Ra=3000$, $Le=5$, $Rm=5000$, $m=0$.

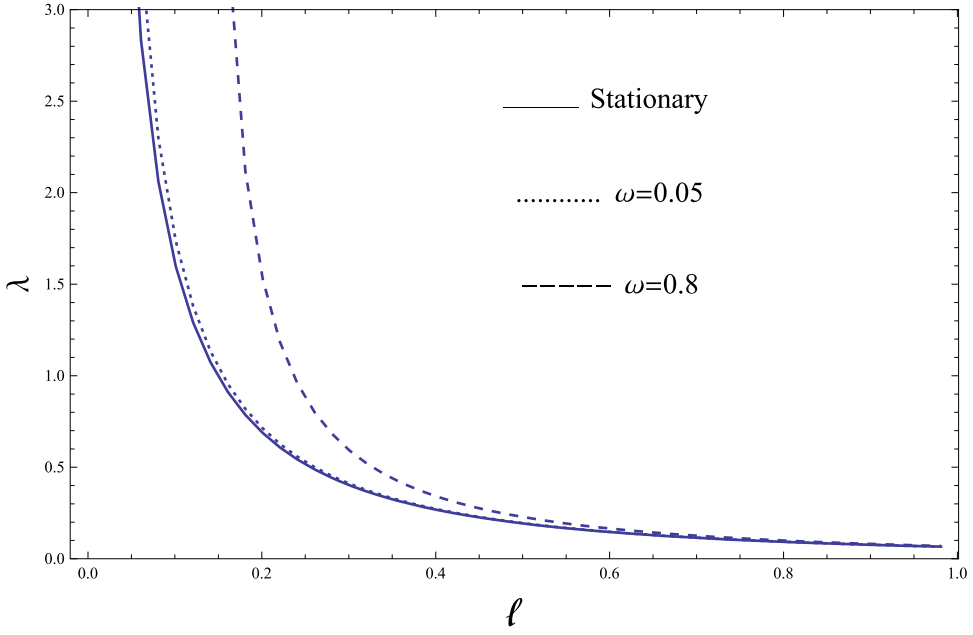

Fig. 8. Stability diagram for a system having the particulars: $Pr=100$, $Rn=300$, $Ra=100$, $Le=100$, $Rm=500$, $m=0.5$.

The particle density stabilizes the nanofluid layer. This occurs due to the stabilizing effect of the concentration Rayleigh number as shown in Fig. 4.

Physically, the large values of the wave number are corresponds to short wave lengths. In other words, for large values of the wave number, the wave length is very small and this induces a stabilized fluid waves. This is illustrated in Fig. 5, where the increasing of the transverse wave number m stabilizes the nanofluid waves.

The results obtained experimentally by Chieruzzi et al. [35] show that the addition of 1.0 wt.% (wt.% means weight percent, i.e. weight of solute/weight of solvent) of nanoparticles to the base salt increases the specific heat of 15% to 57% in the solid phase and of 1% to 22% in the liquid phase. Increasing the specific heat of the nanofluid means a reduction of its ability to heating. In other words, increasing the nanofluid temperature tends to evaporate the fluid easily and provokes higher instabilities of the fluid particles. So, increasing of the specific heat of the base fluid c_f, according to the existence of the nanoparticles, increases the Prandtl number (Pr) and stabilizes the fluid layer as shown in Fig. 6 (due to increasing the stability region).

The modified particle density N_B in Eq. (25) is cancelled due to integration of orthogonal functions. In similar way, the modified diffusivity ratio N_A in Eq. (29) is cancelled due to the determinant expansion. Also, the basic density Rayleigh number R_M is cancelled when applying the restriction of the pressure gradient Eq. (36). This means that the stability analysis is not affect by

the thermophoretic parameter. Meanwhile, the Brownian motion effect appears only through the Lewis number. Increasing of Lewis number destabilizes the motion as shown in Fig. 7.

Another approach to study the stability criteria is obtained by deforming the stationary elasticity parameter λ^S (the real part of Eq. (35)) and oscillatory state of the elasticity parameter λ^{OSC} (as given in Eq. (36)). Fig. 8 illustrates the stationary state λ^S by the solid curve (for zero growth rate $\omega_i = 0$) and the oscillatory state λ^{OSC} (for non-zero growth rate $\omega_i \neq 0$). This figure shows that the oscillatory state departures from the stationary state for a small range of the longitudinal wave number $0 \leq \ell \leq 0.6$. But for higher values of the wave number (short wave length) the fluid becomes stable anywhere (according to conceding the curves for $\ell \geq 0.6$). This confirms the previous result for the transverse wave number m as illustrated before in Fig. 5.

7. Conclusion

In this paper, we have examined the stability of the viscoelastic nanofluid vertical layer. In case of the vertical flow, it is convenient to consider the existence of the vertical streaming velocity at the stationary state. Also, it was expected that the non-Newtonian rheology and the nanoparticles have considerable influence on the stability picture. The solution of the equations of motion along the normal modes technique leads to a cubic dispersion equation with complex coefficients. The main results of our study can be epitomized in the following points:

1. The application of the Routh–Hurwitz stability conditions divides the plane into several stable/unstable parts.
2. The nanofluid of non-Newtonian base is more stable than of Newtonian base.
3. The thermal Rayleigh number stabilizes the nanofluid layer.
4. The stability is restricted by a condition on the pressure gradient (Eq. (36)). This condition gives real values for all Routh–Hurwitz conditions.
5. The particle density stabilizes the nanofluid layer.
6. The Prandtl number (Pr) stabilizes the nanofluid layer due to increasing of the specific heat of the base fluid c_f.

Acknowledgment

The authors would like to bring profound thanks to the reviewers for their venerable efforts and valuable comments that have enriched the article.

Appendix

The constants $c_0 - c_3$ that appear in Eq. (23), may be listed as follows

$$c_0 = \left(\pi^4 + \ell^4 + m^4\right), \quad c_1 = -\frac{1}{2}\frac{\partial P}{\partial y} - \frac{1}{2}R_M + \frac{1}{3}R_a - \frac{1}{6}R_N,$$

$$c_2 = \frac{1}{2}\frac{\partial P}{\partial y} + \frac{1}{2}R_M - \frac{1}{3}R_a, \quad c_3 = \frac{1}{6}R_a + \frac{1}{6}R_N.$$

The constants M_{11}, M_{22} and M_{33} that appear in Eq. (29), may be written as follows

$$M_{11} = i\,a_1\omega + (a_2 + i\,b_2),$$
$$M_{22} = i\,\omega + (a_3 + i\,b_3),$$
$$M_{33} = i\,\omega + (a_4 + i\,b_4).$$

where, the constants $a_1 - a_4$ and $b_2 - b_4$ are given by

$$a_1 = \frac{-1}{2\,\mathrm{Pr}}\delta^2 + \frac{1}{2}\lambda\,c_0^2,$$

$$a_2 = \frac{-1}{2}c_0^2 - \lambda\left(\ell^2 + \ell\,m\right)\left[\delta^2\left(c_1 + c_2 + 6\,c_3\left(\frac{1}{6} - \frac{1}{4\pi^2}\right)\right) + 6\,c_3\right],$$

$$a_3 = \delta^2, \quad a_4 = \frac{1}{Le}\delta^2,$$

$$b_2 = \frac{1}{2}\ell\left(1 - \lambda\,\delta^2\right)(2\,c_2 + 3\,c_3) + \ell\left(\lambda\,c_0^2 - \delta^2\right)\left(\frac{1}{4}c_1 + c_2\left(\frac{1}{6} - \frac{1}{4\pi^2}\right) + c_3\left(\frac{1}{8} - \frac{3}{8\pi^2}\right)\right),$$

$$b_3 = \ell\left[\frac{1}{2}c_1 + \left(\frac{1}{3} - \frac{1}{2\pi^2}\right)c_2 + \left(\frac{1}{4} - \frac{3}{4\pi^2}\right)c_3\right], \quad b_4 = b_3$$

The dispersion relation Eq. (30) coefficients $h_0 - h_3$ and $k_1 - k_3$ are given by

$$h_0 = -a_1, \quad h_1 = -a_1\,b_3 - a_1\,b_4 - b_2,$$
$$h_2 = a_1\,(a_3a_4 - b_3b_4) + a_2\,(a_3 + a_4) - b_2(b_3 + b_4),$$
$$h_3 = a_2\,(a_3b_4 + b_3a_4) + b_2\,(a_3a_4 - b_3b_4),$$
$$k_1 = a_1\,a_3 + a_1\,a_4 + a_2,$$
$$k_2 = a_1\,(a_3b_4 + b_3a_4) + a_2\,(b_3 + b_4) - b_2(a_3 + a_4),$$
$$k_3 = -a_2\,(a_3a_4 - b_3b_4) - b_2\,(a_3b_4 + b_3a_4).$$

The constants $m_1 - m_7$ and $n_1 - n_7$ appearing in Eqs. (34) and (35) are defined as

$$m_1 = \frac{1}{2\,\mathrm{Pr}}\delta^2, \quad n_1 = -\frac{1}{2}c_0^2$$

$$m_2 = \frac{1}{2\,\mathrm{Pr}}\delta^2(a_3 + a_4) + \frac{1}{2}c_0^2,$$

$$n_2 = \frac{-1}{2}c_0^2(a_3 + a_4) + \left(\ell^2 + \ell\,m\right)\left(\delta^2\left(c_1 + c_2 + 6\,c_3\left(\frac{1}{6} - \frac{1}{4\pi^2}\right)\right) - 6\,c_3\right),$$

$$m_3 = \frac{-1}{2\,\mathrm{Pr}}\delta^2(a_3a_4 - b_3b_4) - \frac{1}{2}c_0^2\,(a_3 + a_4) - (b_3 + b_4)\left[\frac{1}{2}\ell\,(2\,c_2 + 3\,c_3) - \ell\,\delta^2\left(\frac{1}{4}c_1 + c_2\left(\frac{1}{6} - \frac{1}{4\pi^2}\right) + c_3\left(\frac{1}{8} - \frac{3}{8\pi^2}\right)\right)\right],$$

$$n_3 = \frac{1}{2}c_0^2(a_3a_4 - b_3b_4) + (a_3 + a_4)\left(\ell^2 + \ell\,m\right) \times\left[-\delta^2\left(c_1 + c_2 + 6\,c_3\left(\frac{1}{6} - \frac{1}{4\pi^2}\right)\right) + 6\,c_3\right] - (b_3 + b_4)\left[-\frac{1}{2}\ell\,\delta^2\,(2\,c_2 + 3\,c_3) + \ell\,c_0^2\left(\frac{1}{4}c_1 + c_2\left(\frac{1}{6} - \frac{1}{4\pi^2}\right) + c_3\left(\frac{1}{8} - \frac{3}{8\pi^2}\right)\right)\right],$$

$$m_4 = -\frac{1}{2}c_0^2(a_3a_4 - b_3b_4) - (a_3b_4 + b_3a_4)\left[\frac{1}{2}\ell\,(2\,c_2 + 3\,c_3) - \ell\,\delta^2\left(\frac{1}{4}c_1 + c_2\left(\frac{1}{6} - \frac{1}{4\pi^2}\right) + c_3\left(\frac{1}{8} - \frac{3}{8\pi^2}\right)\right)\right],$$

$$n_4 = (a_3a_4 - b_3b_4) + \left(\ell^2 + \ell\,m\right) \times\left[-\delta^2\left(c_1 + c_2 + 6\,c_3\left(\frac{1}{6} - \frac{1}{4\pi^2}\right)\right) + 6\,c_3\right] - (a_3b_4 + b_3a_4)\left[-\frac{1}{2}\ell\,\delta^2\,(2\,c_2 + 3\,c_3) + \ell\,c_0^2\left(\frac{1}{4}c_1 + c_2\left(\frac{1}{6} - \frac{1}{4\pi^2}\right) + c_3\left(\frac{1}{8} - \frac{3}{8\pi^2}\right)\right)\right],$$

$$m_5 = \frac{1}{2\,\mathrm{Pr}}\delta^2(b_3+b_4) - \Big[\frac{1}{2}\ell\,(2\,c_2+3\,c_3) - \ell\,\delta^2\Big(\frac{1}{4}c_1 + c_2\Big(\frac{1}{6}-\frac{1}{4\pi^2}\Big) + c_3\Big(\frac{1}{8}-\frac{3}{8\pi^2}\Big)\Big)\Big],$$

$$n_5 = -\frac{1}{2}c_0^2(b_3+b_4) - \Big[-\frac{1}{2}\ell\,\delta^2(2\,c_2+3\,c_3) + \ell\,c_0^2\Big(\frac{1}{4}c_1 + c_2\Big(\frac{1}{6}-\frac{1}{4\pi^2}\Big) + c_3\Big(\frac{1}{8}-\frac{3}{8\pi^2}\Big)\Big)\Big],$$

$$m_6 = \frac{-1}{2\,\mathrm{Pr}}\delta^2(a_3b_4+b_3a_4) + \frac{1}{2}c_0^2\,(b_3+b_4) - (a_3+a_4)\Big[\frac{1}{2}\ell\,(2\,c_2+3\,c_3) - \ell\,\delta^2\Big(\frac{1}{4}c_1 + c_2\Big(\frac{1}{6}-\frac{1}{4\pi^2}\Big) + c_3\Big(\frac{1}{8}-\frac{3}{8\pi^2}\Big)\Big)\Big],$$

$$n_6 = -\frac{1}{2}c_0^2(a_3b_4+b_3a_4) - (b_3+b_4)\,\big(\ell^2+\ell\,m\big) \times\Big[-\delta^2\Big(c_1+c_2+6\,c_3\Big(\frac{1}{6}-\frac{1}{4\pi^2}\Big)\Big)+6\,c_3\Big] - (a_3+a_4)\Big[-\frac{1}{2}\ell\,\delta^2\,(2\,c_2+3\,c_3) + \ell\,c_0^2\Big(\frac{1}{4}c_1 + c_2\Big(\frac{1}{6}-\frac{1}{4\pi^2}\Big) + c_3\Big(\frac{1}{8}-\frac{3}{8\pi^2}\Big)\Big)\Big],$$

$$m_7 = -\frac{1}{2}c_0^2(a_3b_4+b_3a_4) + (a_3a_4-b_3b_4)\Big[\frac{1}{2}\ell\,(2\,c_2+3\,c_3) - \ell\,\delta^2\Big(\frac{1}{4}c_1 + c_2\Big(\frac{1}{6}-\frac{1}{4\pi^2}\Big) + c_3\Big(\frac{1}{8}-\frac{3}{8\pi^2}\Big)\Big)\Big],$$

$$n_7 = (a_3b_4+b_3a_4) + \big(\ell^2+\ell\,m\big) \times\Big[-\delta^2\Big(c_1+c_2+6\,c_3\Big(\frac{1}{6}-\frac{1}{4\pi^2}\Big)\Big)+6\,c_3\Big] + (a_3a_4-b_3b_4)\Big[-\frac{1}{2}\ell\,\delta^2\,(2\,c_2+3\,c_3) + \ell\,c_0^2\Big(\frac{1}{4}c_1 + c_2\Big(\frac{1}{6}-\frac{1}{4\pi^2}\Big) + c_3\Big(\frac{1}{8}-\frac{3}{8\pi^2}\Big)\Big)\Big].$$

References

[1] J. Buongiorno, Convective transport in nanofluids, J. Heat Trans. ASME 128 (2006) 240–250.
[2] J.M. Wu, J. Zhao, A review of nanofluid heat transfer and critical heat flux enhancement – research gap to engineering application, Prog. Nuclear Eng. 66 (2013) 13–24.
[3] M. Mustafa, S. Hina, T. Hayat, A. Alsaedi, Influence of wall properties on the peristaltic flow of a nanofluid: analytic and numerical solutions, Int. J. Heat Mass Trans. 55 (2012) 4871–4877.
[4] T. Hayat, R. Iqbal, A. Tanveer, A. Alsaedi, Influence of convective conditions in radiative peristaltic flow of pseudoplastic nanofluid in a tapered asymmetric channel, J. Magnet. Magn. Mater. 408 (2016) 168–176.
[5] T. Hayat, R. Iqbal, A. Tanveer, A. Alsaedi, Soret and Dufour effects in MHD peristalsis of pseudoplastic nanofluid with chemical reaction, J. Mol. Liq. 220 (2016) 693–706.
[6] T. Hayat, Z. Nisar, H. Yasminb, A. Alsaedi, Peristaltic transport of nanofluid in a compliant wall channel with convective conditions and thermal radiation, J. Mol. Liq. 220 (2016) 448–453.
[7] S.A. Shehzad, F.M. Abbasi, T. Hayat, F. Alsaadi, Model and comparative study for peristaltic transport of water based nanofluids, J. Mol. Liq. 209 (2015) 723–728.
[8] F.M. Abbasi, S.A. Shehzad, T. Hayat, B. Ahmad, Doubly stratified mixed convection flow of Maxwell nanofluid with heat generation/absorption, J. Magnet. Magn. Mater. 404 (2016) 159–165.
[9] J.A. Khan, M. Mustafa, T. Hayat, A. Alsaedi, Three-dimensional flow of nanofluid over a non-linearly stretching sheet: an application to solar energy, Int. J. Heat Mass Trans. 86 (2015) 158–164.
[10] M. Mustafa, J.A. Khan, T. Hayat, A. Alsaedi, On Bödewadt flow and heat transfer of nanofluids over a stretching stationary disk, J. Mol. Liq. 211 (2015) 119–125.
[11] S.A. Shehzad, Z. Abdullah, F.M. Abbasi, T. Hayat, A. Alsaedi, Magnetic field effect in three-dimensional flow of an Oldroyd-B nanofluid over a radiative surface, J. Magnet. Magn. Mater. 399 (2016) 97–108.
[12] A. Alsaedi, M. Awais, T. Hayat, Effects of heat generation/absorption on stagnation point flow of nanofluid over a surface with convective boundary conditions, Commun. Nonlinear Sci. Num. Sim. 17 (2012) 4210–4223.
[13] M. Sheikholeslami, T. Hayat, A. Alsaedi, MHD free convection of Al_2O_3 – water nanofluid considering thermal radiation: a numerical study, Int. J. Heat Mass Trans. 96 (2016) 513–524.
[14] V.K. Andreev, V.B. Bekezhanova, Stability of non-isothermal fluids (review), J. Appl. Mech. Tech. Phys. 54 (2) (2013) 171–184.
[15] C.P. Manosh, D.A.S. Rees, M. Wilson, The influence of higher order effects on the linear wave instability of vertical free convective boundary layer flow, Int. J. Heat Mass Trans. 48 (2005) 809–817.
[16] L.J. Sheu, Linear stability of convection in a viscoelastic nanofluid Layer, World Acad. Sci. Eng.. Tech. 5 (2011) 232–238.
[17] C.F. Fong, K. Walters, The solution of flow problems in the case of materials with memory. II. The stability of plane Poiseuille flow of slightly viscoelastic liquids, J. Mech. 4 (1965) 439–453.
[18] M. Javed, T. Hayat, M. Mustafa, B. Ahmad, Velocity and thermal slip effects on peristaltic motion of Walters-B fluid, Int. J. Heat Mass Trans. 96 (2016) 210–217.
[19] T. Hayat, A. Tanveer, A. Alsaedi, Mixed convective peristaltic flow of Carreau–Yasuda fluid with thermal deposition and chemical reaction, Int. J. Heat Mass Trans. 96 (2016) 474–481.
[20] T. Hayat, S. Farooq, A. Alsaedi, B. Ahmad, Hall and radial magnetic field effects on radiative peristaltic flow of Carreau–Yasuda fluid in a channel with convective heat and mass transfer, J. Magnet. Magn. Mater. 412 (2016) 207–216.
[21] S. Hina, M. Mustafa, T. Hayat, A. Alsaedi, Peristaltic transport of Powell–Eyring fluid in a curved channel with heat/mass transfer and wall properties, Int. J. Heat & Mass Trans. 101 (2016) 156–165.
[22] T. Hayat, H. Zahir, Anum Tanveer, A. Alsaedi, Influences of Hall current and chemical reaction in mixed convective peristaltic flow of Prandtl fluid, J. Magnet. Magn. Mater. 407 (2016) 321–327.
[23] M. Javed, T. Hayat, A. Alsaedi, Peristaltic flow of Burgers' fluid with compliant walls and heat transfer, Appl. Math. Comp. 244 (2014) 654–671.
[24] M. Waqas, T. Hayat, M. Farooq, S.A. Shehzad, A. Alsaedi, Cattaneo-Christov heat flux model for flow of variable thermal conductivity generalized Burgers fluid, J. Mol. Liq. 220 (2016) 642–648.
[25] T. Hayat, M. Ijaz Khan, M. Farooq, A. Alsaedi, M. Waqas, T. Yasmeen, Impact of Cattaneo–Christov heat flux model in flow of variable thermal conductivity fluid over a variable thicked surface, Int. J. Heat Mass Trans. 99 (2016) 702–710.
[26] T. Hayat, T. Muhammad, S.A. Shehzad, A. Alsaedi, On three-dimensional boundary layer flow of Sisko nanofluid with magnetic field effects, Adv. Powder Tech. 27 (2016) 504–512.
[27] S. Hina, M. Mustafa, T. Hayat, N.D. Alotaibi, On peristaltic motion of pseudoplastic fluid in a curved channel with heat/mass transfer and wall properties, Appl. Math. Comp. 263 (2015) 378–391.
[28] T. Hayat, Z. Hussain, M. Farooq, A. Alsaedi, Effects of homogeneous and heterogeneous reactions and melting heat in the viscoelastic fluid flow, J. Mol. Liq. 215 (2016) 749–755.
[29] T. Hayat, S. Bibi, M. Rafiq, A. Alsaedi, F.M. Abbasi, Effect of an inclined magnetic field on peristaltic flow of Williamson fluid in an inclined channel with convective conditions, J. Magnet. Magn. Mater. 401 (2016) 733–745.
[30] T. Hayat, M. Shafique, A. Tanveer, A. Alsaedi, Hall and ion slip effects on peristaltic flow of Jeffrey nanofluid with Joule heating, J. Magnet. Magn. Mater. 407 (2016) 51–59.
[31] D.A. Nield, A.V. Kuznetsov, The onset of convection in a horizontal nanofluid layer of finite depth, Eur. J. Mech. B/Fluids 29 (2010) 217–223.
[32] J.C. Umavathi, Effect of modulation on the onset of thermal convection in a viscoelastic fluid-saturated nanofluid porous layer, Int. J. Eng. Res. Appl. 3 (2013) 923–942.
[33] D.W. Beard, K. Walters, Elastico-viscous boundary-layer flows. I. Two-dimensional flow near a stagnation point, Proc. Camb. Phil. Soc. 60 (1964) 067.
[34] Y. Ishida, T. Yamamoto, Linear and Nonlinear Rotordynamics, Wiley-VCH Verlag, Weinheim, Germany, 2012.
[35] M. Chieruzzi, G.F. Cerritelli, A. Miliozzi, J.M. Kenny, Effect of nanoparticles on heat capacity of nanofluids based on molten salts as PCM for thermal energy storage, Nanoscale Res. Lett. 8 (2013) 448.